Applied Catalysis B: Environmental 168-169 (2015) 293–302

Contents lists available at ScienceDirect

Applied Catalysis B: Environmental

journal homepage: www.elsevier.com/locate/apcatb

The simultaneous selective catalytic reduction of N_2O and NO_X with CH_4 on Co- and Ni-exchanged mordenite

Maria Cristina Campa[a,*], Daniela Pietrogiacomi[a,b], Manlio Occhiuzzi[a]

[a] CNR-Istituto per lo Studio dei Materiali Nanostrutturati, c/o Dipartimento di Chimica, "Sapienza" Università di Roma, Piazzale Aldo Moro 5, 00185 Roma, Italy
[b] Dipartimento di Chimica, "Sapienza" Università di Roma, Piazzale Aldo Moro 5, 00185 Roma, Italy

ARTICLE INFO

Article history:
Received 29 October 2014
Received in revised form
19 December 2014
Accepted 23 December 2014
Available online 27 December 2014

Keywords:
NO abatement by CH_4-SCR
N_2O abatement by CH_4-SCR
NO and N_2O simultaneous abatement by CH_4-SCR
Co-MOR
Ni-MOR

ABSTRACT

Co- or Ni-exchanged Na-MOR (Si/Al = 9.2) prepared by ion-exchange method were characterized by in situ UV–vis DRS and FTIR. We studied the selective catalytic reduction with CH_4 in the presence of O_2 (CH_4-SCR) for the simultaneous abatement of NO and N_2O (CH_4-SCR_{sim}) and the related reactions: (i) abatement of N_2O ($CH_4 - SCR_{N_2O}$), (ii) abatement of NO (CH_4-SCR_{NO}), (iii) N_2O decomposition, and (iv) CH_4 combustion. The catalytic measurements were performed in a flow apparatus with GC analysis of reactants and products.

FTIR characterization with CO of Ni-MOR identified isolated Ni^{2+} and [Ni^{2+}—O—Ni^{2+}] dimers, both mainly located in α-sites. In Ni-MOR, the amount of isolated Ni^{2+} and of dimers was comparable, whereas in Co-MOR isolated Co^{2+} were more abundant than [Co^{2+}—O—Co^{2+}]. Transition metal ion (tmi) dimers were easily reduced by CO to [tmi^{+}—□—tmi^{+}] yielding CO_2. In situ UV–vis DRS characterization indicated that by heating in N_2O, Co^{2+} oxidized to Co^{3+}—O^{-}, whereas Ni^{2+} did not.

Catalytic results for CH_4-SCR_{sim} showed that Co-MOR was active, whereas Ni-MOR was ineffective, because it did not abate N_2O. Both catalysts were active for $CH_4 - SCR_{N_2O}$ and for CH_4-SCR_{NO}. Whereas Co-MOR was highly active for N_2O decomposition and poorly active for CH_4 combustion, Ni-MOR was inactive for N_2O decomposition and active for CH_4 combustion.

The NO abatement in CH_4-SCR_{sim} on both Co-MOR and Ni-MOR occurred via CH_4-SCR_{NO}, and the active sites were isolated tmi^{2+} in α-sites. The N_2O abatement in CH_4-SCR_{sim} on Co-MOR occurred in β-sites via N_2O decomposition, and the active sites were isolated Co^{2+}, that formed Co^{3+}—O^{-} intermediate (UV–vis DRS evidence). The N_2O abatement in CH_4-SCR_{sim} on Ni-MOR did not occur, because Ni^{2+}, that formed no Ni^{3+}—O^{-}, were inactive in N_2O decomposition. Redox behavior of [Ni^{2+}—O—Ni^{2+}] accounted for Ni-MOR activity in $CH_4 - SCR_{N_2O}$ and CH_4 combustion.

1. Introduction

A challenge in environment protection is the abatement of harmful NO_x emissions and of greenhouse gases as N_2O, whose global warming potential is about 300 times higher than that of CO_2 [1]. In nitric acid plants EnviNOx® process performs the tail-gas abatement of NO_x and N_2O over iron containing zeolite catalysts in two catalytic beds [2], where NO_x was abated by NH_3, and N_2O by hydrocarbons or via decomposition [3]. It would be favorable to reduce both the pollutants in one catalytic bed, using the same reducing agent as natural gas. Thus far, few papers were addressed to simultaneous selective catalytic reduction with hydrocarbons in a double catalytic bed [4–7], or in a single catalytic bed [8,9]. When a single catalyst was adopted for the simultaneous abatement, it was suggested that the nitrogen oxides partially competed for the same active sites [9].

Transition metal ions (tmi) in zeolites have been extensively investigated for the abatement of nitrogen oxides [10–14]. Co-MOR catalysts are active for the selective catalytic reduction of NO with CH_4 in the presence of excess O_2 (CH_4-SCR_{NO}) [15–18], and for the selective catalytic reduction of N_2O with CH_4 in the presence of excess O_2 ($CH_4 - SCR_{N_2O}$) [19]. We therefore proposed Co-MOR as a potential catalyst, on one catalytic bed, for the simultaneous abatement of both N_2O and NO using CH_4 as the reducing agent in the presence of excess O_2 (CH_4-SCR_{sim}) [19]. In agreement with this prevision, preliminary results on an extensively exchanged

* Corresponding author. Fax: +39 6 490324.
E-mail address: mariacristina.campa@uniroma1.it (M.C. Campa).

http://dx.doi.org/10.1016/j.apcatb.2014.12.040
0926-3373/

Co-MOR sample (104% of exchange) showed that this catalyst was active for the CH_4-SCR_{sim} process [20].

Ni-MOR catalysts are active for both CH_4-SCR_{NO} [11,21,22] and $CH_4 - SCR_{N_2O}$ [21,23]. Our previous investigation on $CH_4 - SCR_{N_2O}$ in Ni-, Co- and Fe-MOR showed that these catalysts were active in the order Fe-MOR > Ni-MOR > Co-MOR, with CO_2 selectivity about 100% on Ni-MOR. We inferred that Ni-MOR, being active for the $CH_4 - SCR_{N_2O}$ and for the CH_4-SCR_{NO} and forming no CO, were promising catalysts for CH_4-SCR_{sim} [23].

In this paper we extended the study on CH_4-SCR_{sim} to Co-MOR samples at various Co-exchange extent, from 11 to 104%, and to Ni-MOR at Ni-exchange extent 20–80%. All catalysts were prepared by ion-exchange of Na-MOR. The Co-MOR samples were portions of those we have previously characterized [15,24,25]. Ni-MOR and Co-MOR were characterized by in situ UV–vis DRS and FTIR to investigate tmi nuclearity, coordination and redox properties. To clarify the role of these key factors influencing the catalytic activity and directing the reaction pathway, we correlated the characterization results with the catalytic behavior for CH_4-SCR_{sim} and related reactions ($CH_4 - SCR_{N_2O}$, CH_4-SCR_{NO}, N_2O decomposition, and CH_4 combustion).

2. Experimental

2.1. Catalysts

Co-MOR and Ni-MOR catalysts (Table 1) were prepared by ion-exchange of Na-MOR (Si/Al = 9.2, Tosoh Corporation). In Na-MOR samples, the analytical Na content equaled the Al content calculated from the analytical Si/Al ratio given by the supplier (Na^+/Al = 1.05). Details on the MOR matrix are reported in full in a previous paper [24]. Tmi-containing samples were ion-exchanged by contacting a weighted amount of Na-MOR with an aqueous solution of $Co(CH_3COO)_2$ or $Ni(NO_3)_2$ (0.002–0.06 M) for 6 h under stirring at 350 K. To obtain extensively exchanged samples, up to three exchange procedures were run in sequence. After the exchange procedure, samples were thoroughly washed with distilled water, and dried overnight at 383 K (called hereafter as prepared samples).

The sodium, the cobalt and the nickel content of wet samples (equilibrated at ca. 79% relative humidity over a saturated solution of NH_4Cl) were determined by atomic absorption (Varian SpectrAA-220), and expressed as Na^+/Al and $2tmi^{2+}$/Al ratios, where tmi is the Co or Ni exchanged. Exchanged samples are labeled as tmi-MOR-*a*, where *a* is the analytical tmi-exchange percentage (Table 1).

2.2. Catalytic experiments

The catalytic activity was measured in a flow apparatus at atmospheric pressure. The apparatus included a feeding section where five gas streams (He, 3% N_2O in He, 3% NO in He, 1.5% CH_4 in He, 10% O_2 in He) were regulated by means of independent mass flow controller-meters (MKS) and mixed in a glass ampoule before entering the reactor. Gas mixtures were purchased from Rivoira and used without further purification. The reactor was made of silica with an internal sintered frit of about 12 mm diameter supporting the powdered catalyst. Reactants and products were analyzed by a gas-chromatograph (Agilent 7890 A GC system) equipped with three columns (Molsieve 5 A, for detecting O_2, N_2 and CO, Porapack Q for detecting CO_2 and N_2O, and Na_2SO_4-doped alumina for detecting CH_4) and two detectors (TCD and FID). Experiments yielded satisfactory nitrogen and carbon balances.

A portion of as prepared sample (0.1 g) was treated in a flow of 2.5% O_2/He mixture (100 $cm^3\,min^{-1}$), while the reactor was heated from RT to 773 K in about 45 min and then isothermally at 773 K for 90 min. After this treatment, the reactor was bypassed and the temperature adjusted to the desired value. The reaction temperature was changed at random without intermediate activation treatment. For all reactions, the catalyst was stable as a function of the time on stream, throughout experiments lasting up to about 8 h. The total flow rate was maintained at 50 cm^3 STP/min, and space velocity (GHSV) was 15,000 h^{-1}, based on the apparent sample density of 0.5 $g\,cm^{-3}$. Conversions obtained at various (sample weight)/(flow rate) ratios (W/F) indicated that, in our conditions, reaction is under kinetic control without diffusion effect. Catalysis was run by contacting the catalyst with mixtures of various composition (v/v, He as balance): N_2O:CH_4:O_2 (4000:4000:20000 ppm), NO:CH_4:O_2 (4000:4000:20000 ppm), N_2O:NO:CH_4:O_2 (4000:4000:4000:20000 ppm), CH_4:O_2 (4000:20000 ppm), and N_2O (4000 ppm),

Percent N_2O or CH_4 conversion was calculated from (molecules-consumed)/(molecules-injected). Percent NO conversion was calculated from ($2N_2$ produced)/(NO injected). The percent CH_4 amount reacting with N_2O in the simultaneous abatement (ξ) was calculated from (CH_4 conversion in CH_4-SCR_{sim} − CH_4 conversion in CH_4-SCR_{NO}). The percent CO_2 selectivity (CO_2 rather than CO) was calculated as (CO_2 formed)/(CO_2 + CO) molecules-formed). For each catalyst, reaction rate (R/molecules $s^{-1}\,g^{-1}$) of NO or N_2O or CH_4 consumption and apparent activation energy values (E_a/kJ mol^{-1}) were calculated from experiments in which conversion values did not exceed 30% ($\log R$ vs. $1/T$).

2.3. Characterization techniques

IR spectra were run at room temperature (RT) on an FTIR spectrometer (PerkinElmer Frontier) equipped with a MCT detector, operating at a resolution of 4 cm^{-1}. The powdered as prepared samples were pelleted (pressure, 2×10^4 $kg\,cm^{-2}$) in self-supporting disks of ca. 10 $mg\,cm^{-2}$, and put in an IR cell which allowed thermal treatments in vacuum or in a controlled atmosphere. Infrared spectra were run in situ on samples either (i) heated with O_2 (100 Torr) at 773 K for 1 h and evacuated at the same temperature for 1 h (called hereafter standard activated) or (ii) standard activated, contacted with CO (100 Torr, SOL, 99.9%) at RT and heated in CO at increasing temperature up to 623 K, for 10 min at each temperature. Before recording spectra, all samples were cooled in CO at RT. For band integration and curve fitting, we used the software program "Curvefit in Spectra Calc." (Galactic Industries).

In situ UV–vis DRS spectra were recorded at RT in the wavenumber range of 4000–50000 cm^{-1} using a Varian Cary 5 E spectrometer (software Cary Win UV). The spectra were run in situ in a quartz cell with optical windows, that allowed thermal treatments in vacuum or in a controlled atmosphere. The spectra were recorded on samples (about 1.0 g) (i) as-prepared in air, (ii) standard activated, (iii) standard activated, heated in CO at increasing temperature up to 623 K and cooled in CO at RT, and iv) standard activated and heated in N_2O

Table 1
Cobalt- or nickel-exchanged MOR: analytical cobalt, nickel, and sodium amounts.

Catalysts	Na^+/Al	$2tmi^{2+}$/Al[a]
Co-MOR-11	0.91	0.11
Co-MOR-23	0.79	0.23
Co-MOR-73	0.32	0.73
Co-MOR-104	0.28	1.04
Ni-MOR-20	0.75	0.20
Ni-MOR-80	0.24	0.80

[a] tmi^{2+}/Al is Ni^{2+}/Al, or Co^{2+}/Al, depending on the catalyst.

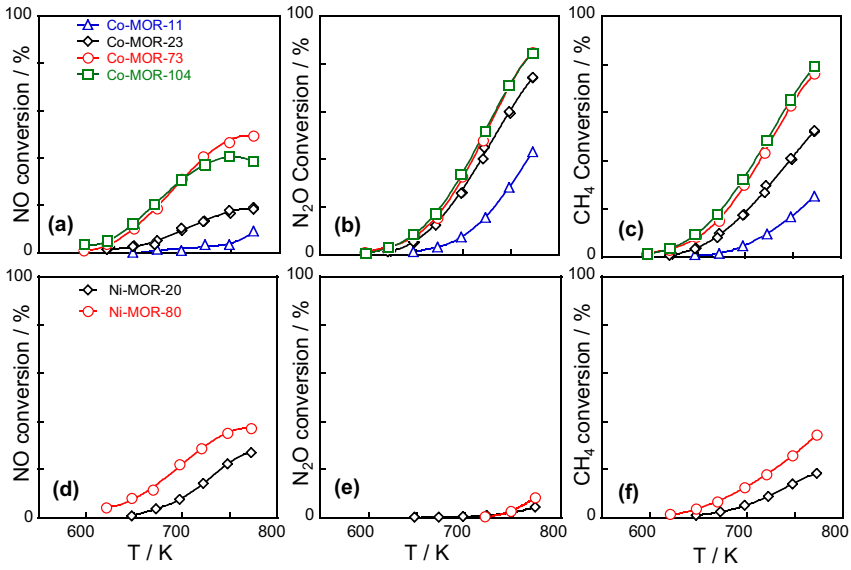

Fig. 1. CH_4-SCR_{sim} reaction on tmi-MOR catalysts: percent NO, N_2O and CH_4 conversions as a function of temperature on Co-MOR (Sections a–c) and Ni-MOR (Sections d–f). Catalysts as indicated.

(120 Torr, SOL, 99.9%) at increasing temperature up to 723 K, for 10 min at each temperature, and cooled in N_2O at RT.

3. Results and discussion

3.1. The catalytic activity of Co-MOR and Ni-MOR samples

3.1.1. CH_4-SCR_{sim}

Co-MOR catalysts were active for the CH_4-SCR_{sim} process in the temperature range from 573 to 773 K (Fig. 1a–c), in agreement with previous results on Co-MOR-104 [20]. NO and CH_4 conversions increased on increasing the Co-exchange percentage up to 73% (Fig. 1a and c), whereas N_2O conversion proportionally increased up to 23% of Co-exchange percentage, and little increased at higher Co-content (Fig. 1b). On Co-MOR-73 NO, N_2O and CH_4 conversions were nearly similar to those on Co-MOR-104.

Ni-MOR samples were ineffective for CH_4-SCR_{sim} (Fig. 1d–f). In fact, Ni-MOR-20 and Ni-MOR-80 in the simultaneous abatement were inactive for N_2O reduction (Fig. 1e), even though they were active for NO abatement in the whole temperature range (Fig. 1d). On increasing Ni-content, NO and CH_4 conversions increased (Fig. 1d and f).

In all Co-MOR and Ni-MOR, CO_2 selectivity in the whole temperature range was nearly 100%.

3.1.2. $CH_4 - SCR_{N_2O}$, CH_4-SCR_{NO}, N_2O decomposition, and CH_4 combustion

To provide information on the reaction pathway of the simultaneous process, the catalytic activity in the reactions related to CH_4-SCR_{sim} ($CH_4 - SCR_{N_2O}$, CH_4-SCR_{NO}, N_2O decomposition, and CH_4 combustion) was investigated. In agreement with previous results [15,19,23,25], both low-extent exchanged (Co-MOR-11 and Co-MOR-23) and extensively exchanged samples (Co-MOR-73 and Co-MOR-104) were active for $CH_4 - SCR_{N_2O}$ and for CH_4-SCR_{NO}, highly active for N_2O decomposition (Fig. 2), and poorly active for CH_4 combustion (Fig. 3). On extensively exchanged samples in CH_4-SCR_{sim} the NO conversion equaled that in the CH_4-SCR_{NO} and the N_2O conversion equaled that in the $CH_4 - SCR_{N_2O}$. On this basis, in our preliminary study on Co-MOR-104 [20], we suggested that the simultaneous abatement consisted of the two independent processes: $CH_4 + N_2O + O_2$ and $CH_4 + NO + O_2$. At variance with extensively exchanged samples, on low-extent exchanged catalysts NO and N_2O conversions in CH_4-SCR_{sim} did not strictly match the conversions measured in CH_4-SCR_{NO} and in $CH_4 - SCR_{N_2O}$ (compare Fig. 2c and d with Fig. 2a and b). Besides, on all Co-MOR, although in CH_4-SCR_{sim} N_2O abated was comparable to that abated in $CH_4 - SCR_{N_2O}$ (compare closed squares with open squares in Fig. 2), the CH_4 consumed was lower than that in $CH_4 - SCR_{N_2O}$ (compare open squares with closed circles in Fig. 3). To check the hypothesis of the two independent processes, we compared the CH_4 conversion in simultaneous abatement with those in CH_4-SCR_{NO} and in $CH_4 - SCR_{N_2O}$ (Fig. 3). If the hypothesis was true, the CH_4 conversion in CH_4-SCR_{sim} should be the sum of CH_4 conversions in the two separate abatements. Conversely, for each Co-MOR in the

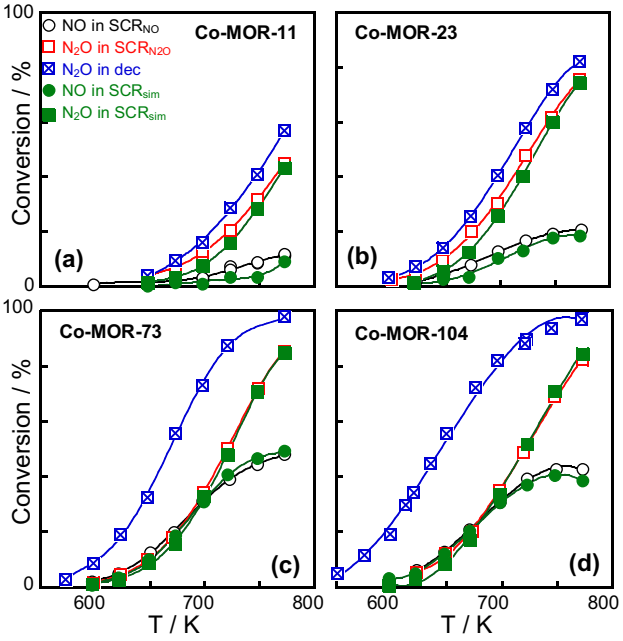

Fig. 2. Comparison between CH_4-SCR_{sim} and related reactions (CH_4-SCR_{NO}, $CH_4 - SCR_{N_2O}$ and N_2O decomposition) on Co-MOR. Percent NO and N_2O conversions as a function of temperature on Co-MOR-11 (Section a), Co-MOR-23 (Section b), Co-MOR-73 (Section c), and Co-MOR-104 (Section d). Reactions as indicated.

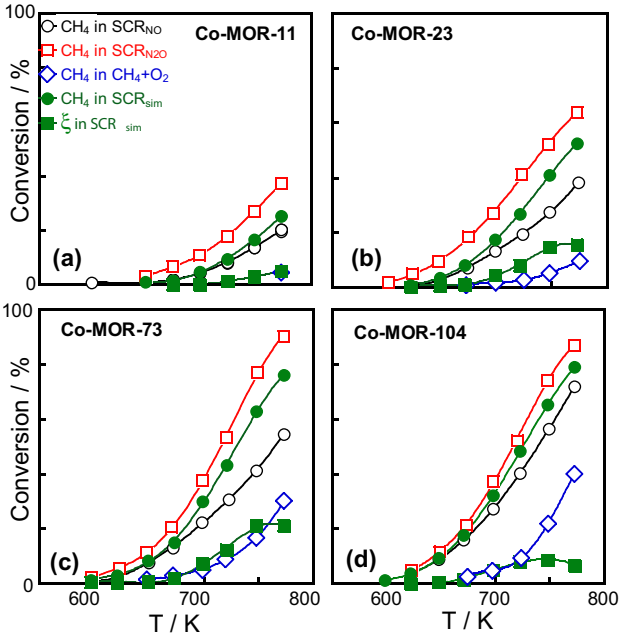

Fig. 3. Comparison between CH_4-SCR_{sim} and related reactions (CH_4-SCR_{NO}, $CH_4 - SCR_{N_2O}$ and CH_4 combustion) on Co-MOR. Percent CH_4 conversion as a function of temperature on Co-MOR-11 (Section a), Co-MOR-23 (Section b), Co-MOR-73 (Section c), and Co-MOR-104 (Section d). Reactions as indicated. Percent amount ξ (■) is calculated as difference between CH_4 conversion in CH_4-SCR_{sim} (●) and CH_4 conversion in CH_4-SCR_{NO} (○).

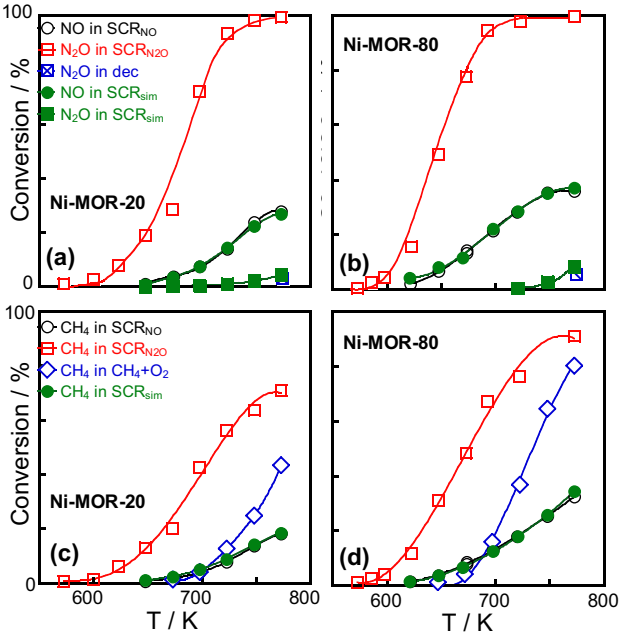

Fig.4. Comparison between CH_4-SCR_{sim} and related reactions (CH_4-SCR_{NO}, $CH_4 - SCR_{N_2O}$, N_2O decomposition and CH_4 combustion) on Ni-MOR. Percent NO and N_2O conversion (Sections a and b) and percent CH_4 conversion (Sections c and d) as a function of temperature. Catalysts and reactions as indicated.

whole range of temperature the CH_4 conversion for the simultaneous abatement had values much lower than the sum (Fig. 3). Taking into account that Co-MOR was inactive for NO decomposition [26] and highly active for N_2O decomposition, we confirmed that in CH_4-SCR_{sim} NO was reduced via CH_4-SCR_{NO}, and hypothesized that N_2O was abated via decomposition. To verify this hypothesis, we calculated the CH_4 amount that reacted with N_2O in simultaneous abatement. This percent amount, hereafter indicated as ξ, was equal to (CH_4 conversion in CH_4-SCR_{sim} − CH_4 conversion in CH_4-SCR_{NO}). In all Co-MOR the ξ value was equal to zero up to about 673 K, and it little increased at higher temperature (closed squares in Fig. 3). This result indicated that up to about 673 K no CH_4 reacted with N_2O and N_2O was abated via decomposition, and that above 673 K a negligible methane amount reacted with N_2O yielding also $CH_4 - SCR_{N_2O}$.

Ni-MOR catalysts were active for both $CH_4 - SCR_{N_2O}$ and CH_4-SCR_{NO}, whereas, at variance with Co-MOR, they were inactive for N_2O decomposition and highly active for CH_4 combustion (Fig. 4). In CH_4-SCR_{sim} on both Ni-MOR-20 and Ni-MOR-80, NO and CH_4 conversions were in the whole temperature range similar to those in CH_4-SCR_{NO}, and N_2O conversion was negligible up to 773 K, whereas it was high in $CH_4 - SCR_{N_2O}$ (Fig. 4). These results indicated that NO was abated via CH_4-SCR_{NO} and that CH_4 did not react with N_2O (Fig. 4). In agreement, the ξ values in the whole temperature range were equal to zero (data not reported for brevity).

These findings confirmed the hypothesis that on tmi-MOR N_2O decomposition had a key role for N_2O abatement in CH_4-SCR_{sim}. On this basis, at variance with Co-MOR, Ni-MOR catalysts were inactive for N_2O abatement in CH_4-SCR_{sim}, because they did not decompose N_2O.

3.2. FTIR characterization

In situ FTIR spectroscopy have been used to investigate the exchange process, the site population, the nuclearity and the reducibility of tmi.

3.2.1. Brønsted acid sites of standard activated samples

Whereas the spectra of low-extent exchanged tmi-MOR (Co-MOR-23 and Ni-MOR-20) showed only the narrow band of terminal silanol on the external surface of the matrix (3740 cm^{-1} [27]), the spectra of extensively exchanged samples (Co-MOR-73 and Ni-MOR-80) showed also the band of Brønsted acid hydroxyls located at the exchanging sites inside the zeolite channels (3615 cm^{-1} [27]) (Fig. 5). As already suggested for Co-MOR at various Co-exchange extent from 11 to 104% [24,28] and for Ni-zeolites [23,29], the thermal treatment subsequent to the exchange process induced the hydrolysis of the anchored $tmi^{2+}(H_2O)_n$ complexes, yielding Brønsted acid hydroxyls and $[tmi(OH)]^+$. On low-extent exchanged tmi-MOR, $tmi^{2+}(H_2O)_n$ were stabilized by the presence of two Al atoms within a specified distance of each other (Al–Al pair). On extensively exchanged tmi-MOR, some $tmi^{2+}(H_2O)_n$ hydrolyzed,

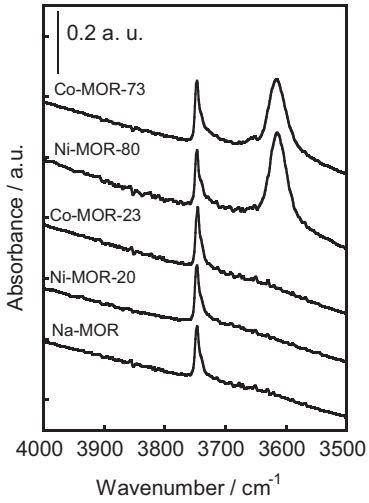

Fig. 5. FTIR spectra of standard activated Na-MOR, Co-MOR and Ni-MOR in the OH stretching region. Catalysts as indicated. Spectra of Co-MOR-23 and Co-MOR-73 from [24].

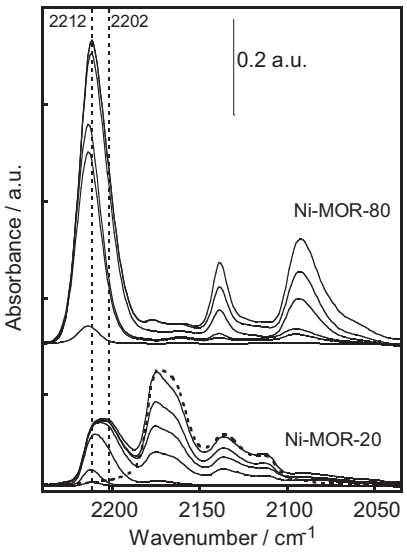

Fig. 6. FTIR spectra of CO adsorbed at RT on standard activated Ni-MOR-20 and Ni-MOR-80 at increasing equilibrium pressure (from 0.050 to 100 Torr). For the sake of comparison, CO adsorbed at RT (100 Torr) on standard activated Na-MOR is reported as a dotted spectrum.

yielding monovalent species stabilized in proximity of isolated Al atoms, being not enough Al–Al pairs [30]. The amount of Brønsted acid hydroxyls in Ni-MOR-80 was similar to that in Co-MOR-73 (Fig. 5). In a previous paper on Co-MOR [24] we calculated that this amount corresponded to about 20% of exchanging sites.

3.2.2. CO adsorption on standard activated samples

On Na-MOR matrix the CO adsorption at RT (dotted line in Fig. 6) yielded the well-known bands due to CO on Na^+ in the main channels (2176 cm^{-1}) and in the side pockets (2163 cm^{-1}) [15,27], to CO multiple interaction (2135 cm^{-1}) [31,32], and to CO adsorbed via the O atom on Na^+ in the main channels (2112 cm^{-1}) [33].

On Co-MOR the CO adsorption at RT have been previously investigated [15]. By FTIR two types of linear Co^{2+}—CO were identified, the first type, the most abundant, occupied the α-sites in the mordenite main channels, and the second one the β-sites in the mordenite smaller channels.

On Ni-MOR samples the CO adsorption, in addition to the matrix bands, yielded absorptions due to Ni—carbonyls (Fig. 6). On Ni-MOR-20 at low CO pressure (<0.5 Torr) a band at 2212 cm^{-1} formed. Increasing CO pressure, the Na^+ carbonyl bands (2176, 2165, 2135, and 2110 cm^{-1}) formed, and the previous band at 2212 cm^{-1} broadened arising a second component at 2202 cm^{-1}. The intensity of the broad band increased with increasing CO pressure and at a pressure of about 100 Torr the band maximum shifted to an intermediate value of about 2207 cm^{-1}, suggesting a similar contribution of the two components. The composite band was assigned to linear Ni^{2+}—CO species with different σ-bond character [34–38]). On Ni-MOR-80 (i) Na^+ carbonyl bands had very low intensity, due to the low Na^+ content, (ii) Ni^{2+}—CO band was more intense than on Ni-MOR-20, and (iii) at CO pressure of about 100 Torr the maximum of the asymmetric band was at 2212 cm^{-1}, suggesting a prevalent contribution of the component at higher wavenumber. On Ni-MOR-80, otherwise from Ni-MOR-20, in addition to Ni^{2+}—CO band, absorptions at 2350 (not shown), 2137 and 2092 cm^{-1} were detected (Fig. 6). The band at 2350 cm^{-1} was due to adsorbed CO_2, and those at 2137 and 2092 cm^{-1} to Ni^+—$(CO)_2$ species (ν_{sym} and ν_{asym}, respectively [38]). The formation of Ni^+ reduced species were induced by the stability of the Ni^+-$(CO)_2$ complex, and it has been reported on Ni-ZSM-5 [34–36], Ni-BEA [39], and Ni-MOR [37,38] systems.

To identify the Ni^{2+}—CO species yielding the composite band at 2212–2202 cm^{-1}, we took into account that in MOR zeolite tmi^{2+} occupy cationic sites with different coordination to framework oxygen atoms: the less coordinated sites are in the main channels, and the more coordinated ones are in side pockets and in secondary channels [16,40]. Lower coordination of tmi^{2+} to framework oxygen atoms induces an higher electrophilic character. Consequently, less coordinated tmi-carbonyls had an higher σ-bond character and an higher wavenumber with respect to more coordinated ones [34,35]. Analogously to Co-MOR [15], we therefore assigned the component at higher wavenumber, 2212 cm^{-1}, to Ni^{2+}—CO in less coordinated α-sites and the component at lower wavenumber, 2202 cm^{-1}, to Ni^{2+}—CO in more coordinated β-sites. On both Ni-MOR samples evacuation at RT caused the preferential decrease of the component at 2202 cm^{-1} with respect to that at 2212 cm^{-1} (spectra not shown), indicating the higher stability of carbonyls in main channels, in agreement with its higher σ-bond character.

As already found on Co-MOR [14], also on Ni-MOR the total amount of Ni^{2+}—CO, evaluated from the integrated-intensity (area/cm^{-1}) of the composite band, increased proportionally on increasing Ni-content (4.1 on Ni-MOR-20 and 15.5 on Ni-MOR-80), suggesting that all tmi were exposed. On both Co-MOR and Ni-MOR, the evaluation of the relative amount of carbonyls in the two sites as a function of the tmi-exchange extent gave information on tmi-exchange process and site population. In previous paper [15], we analyzed for Co-MOR-41, Co-MOR-61 and Co-MOR-89 the amount of Co^{2+}—carbonyls in α-sites and in β-sites by curve fitting, assuming that the position and FWHM of the components remained unchanged. We extended this analysis (curve fittings not reported for brevity) to the Co-MOR and to Ni-MOR samples investigated in the present paper and the results are here reported in full (Fig. 7). In Co-MOR the amount of Co^{2+}-CO in β-sites (integrated intensity, I_β /cm^{-1}) increased with increasing Co-content up to Co-exchange percentage of 23% and then remained nearly constant, whereas the amount of Co^{2+}—CO in α-sites (I_α /cm^{-1}) little increased up to 23%, and linearly increased at higher Co-content. On Ni-MOR-20 the integrated intensity of Ni^{2+}—CO band in α-sites was similar to that in β-sites, whereas on Ni-MOR-80 I_α was much higher than I_β (Fig. 7). On both tmi-MOR, increasing tmi content yielded an increase of the I_α/I_β ratio, namely in the exchange-process tmi firstly occupied β-sites, in agreement with UV–vis DRS characteri-

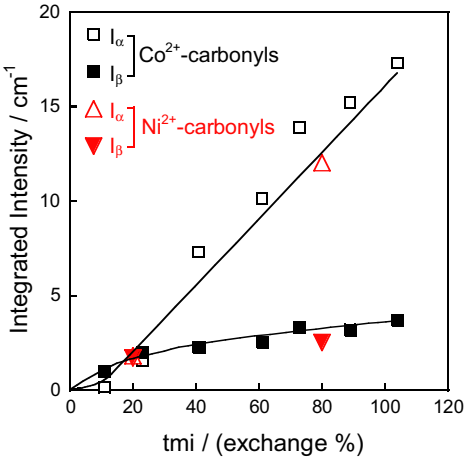

Fig. 7. Integrated intensity of tmi^{2+}—carbonyl bands as a function of tmi-exchange percent. Co^{2+}— and Ni^{2+}—carbonyls in α-sites (I_α /cm^{-1}) and in β-sites (I_β /cm^{-1}), as indicated. Data for Co-MOR-41, Co-MOR-61 and Co-MOR-89 from [15].

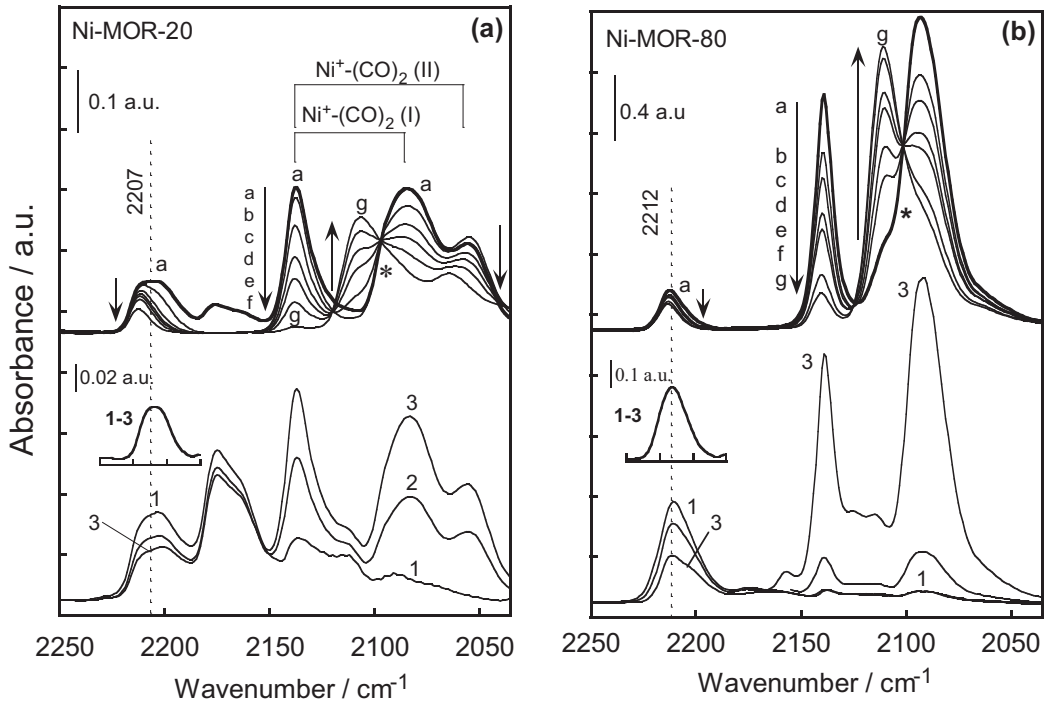

Fig. 8. FTIR spectra of CO adsorbed on Ni-MOR heated in CO at increasing temperature (spectra 1–3), and then degassed at RT at increasing evacuation time (spectra a–g). Ni-MOR-20 (Section a) and Ni-MOR-80 (Section b) heated in CO (100 Torr), at RT (spectrum 1), 523 K (spectrum 2), 623 K (spectrum 3) and then evacuated at RT for increasing time, from 2 to 60 min (spectra a–g). The asterisk indicates the isosbestic point. The insets report the difference between spectrum 3 and spectrum 1 (3–1) in the Ni^{2+}—carbonyl region for Ni-MOR-20 (inset in Section a) and Ni-MOR-80 (inset in Section b).

zation of Co-MOR [41] and with computational results on Ni-MOR [42]. On extensively exchanged tmi-MOR, α-sites are populated in much higher amount than β-sites.

3.2.3. *CO adsorption on samples heated in CO at increasing temperature*

On Co-MOR the CO adsorption on samples heated in CO at increasing temperature have been previously investigated [24]. By FTIR we suggested that heating as prepared extensively exchanged Co-MOR samples (above 60% of Co-exchange) caused the condensation of the adjacent Co–hydroxo complexes with water elimination, so that $[Co—O—Co]^{2+}$ species formed. By heating in CO dimers reduced, whereas isolated Co^{2+} did not. The most abundant species were isolated Co^{2+} ions, being the dimers amount at maximum 14% in Co-MOR-104.

On both Ni-MOR samples, after heating in CO at increasing temperature (from RT to 623 K), CO adsorption formed Ni^{2+}—CO, Ni^{+}—$(CO)_2$ and CO_2 species. Increasing the reduction temperature, the intensity of bands due to Ni^{+}—$(CO)_2$ and CO_2 increased, yielding a maximum at 623 K, whereas the intensity of Ni^{2+}—CO band decreased in parallel (Fig. 8a and b, spectra 1–3). The simultaneous formation of Ni^{+}—$(CO)_2$ and CO_2 species indicated that a small amount of Ni^{2+} underwent reduction by reaction of CO with a labile extra-lattice O atom, suggesting that Ni^{+} originated from $[Ni^{2+}—O—Ni^{2+}]$ dimers that yielded $[(CO)_2Ni^{+}—□—Ni^{+}(CO)_2]$ and CO_2. The decrease of Ni^{2+}—CO band suggested that this band disguised that of $[CO—Ni^{2+}—O—Ni^{2+}—CO]$. The component of the Ni^{2+}—CO band that remained up to 623 K was due to carbonyls on isolated Ni^{2+}, that did not reduce.

On Ni-MOR-80 weak components at 2157, 2125 and 2115 cm^{-1}, already assigned to Ni^{+}—$(CO)_3$ species [38], also formed (Fig. 8b), whereas on Ni-MOR-20 a new broad absorption at 2054 cm^{-1} was detected (Fig. 8a). To assign the band at 2054 cm^{-1}, we investigated the species stability by evacuating the samples at RT for increasing time (Fig. 8a and b, spectra a–g). In both Ni-MOR, on decreasing CO pressure, the band intensity of Ni^{2+}—CO and that of ν_{sym} and ν_{asym} of Ni^{+}—$(CO)_2$ decreased and a new component at about 2110 cm^{-1} in parallel increased. This latter band was assigned to the linear Ni^{+}—CO arising from Ni^{+}—$(CO)_2$ [35], in agreement with the isosbestic point at about 2100 cm^{-1} showing their interconversion (asterisk in Fig. 8a and b).

In Ni-MOR-20, on decreasing CO pressure, the intensity of the band at 2054 cm^{-1} decreased and a new component at 2064 cm^{-1} was detected. We suggest that the band at 2054 cm^{-1} was due to ν_{asym} of a second type of Ni^{+}—$(CO)_2$ species, yielding a second linear Ni^{+}—CO at 2064 cm^{-1} on evacuation. The ν_{sym} of the second type of Ni^{+}—$(CO)_2$ occurred at the same wavenumber as the ν_{sym} of the first type of Ni^{+}—$(CO)_2$ at 2137 cm^{-1}. This suggestion was consistent with the markedly higher intensity-ratio between the two stretching bands at 2137 and 2092 cm^{-1} on Ni-MOR-20 than on Ni-MOR-80. Hereafter, we will refer to Ni^{+}—$(CO)_2$ having ν_{asym} at 2092 cm^{-1} and ν_{sym} at 2137 cm^{-1} as type I Ni^{+}—$(CO)_2$ and that with ν_{asym} at 2054 cm^{-1} and ν_{sym} at about 2137 cm^{-1} as type II Ni^{+}—$(CO)_2$. The relative amount of the two types of Ni^{+}—$(CO)_2$ depended on Ni content: on Ni-MOR-80 the type I was the most abundant (Fig. 8b). These two types of Ni^{+}—$(CO)_2$ arose from two types of $[(CO)—Ni^{2+}—O—Ni^{2+}—(CO)]$. We can roughly evaluate the stretching frequency of the Ni^{2+}—carbonyls belonging to the two types of $[(CO)—Ni^{2+}—O—Ni^{2+}—(CO)]$ from the spectrum obtained as difference between the spectrum of CO adsorbed on the standard activated sample and that after reduction in CO at 623 K. In Ni-MOR-80 the difference spectrum yielded a symmetrical band centered at 2212 cm^{-1} (inset in Fig. 8b), a position similar to that of isolated Ni^{2+}—CO carbonyls in α-sites, whereas in Ni-MOR-20 the difference spectrum was a broad band centered at 2207 cm^{-1} (inset in Fig. 8a), a position similar to that of isolated Ni^{2+}—CO carbonyls in α- and β-sites. The two types of $[(CO)—Ni^{2+}—O—Ni^{2+}—(CO)]$ appeared at nearly the same wavenumber of the two types of isolated

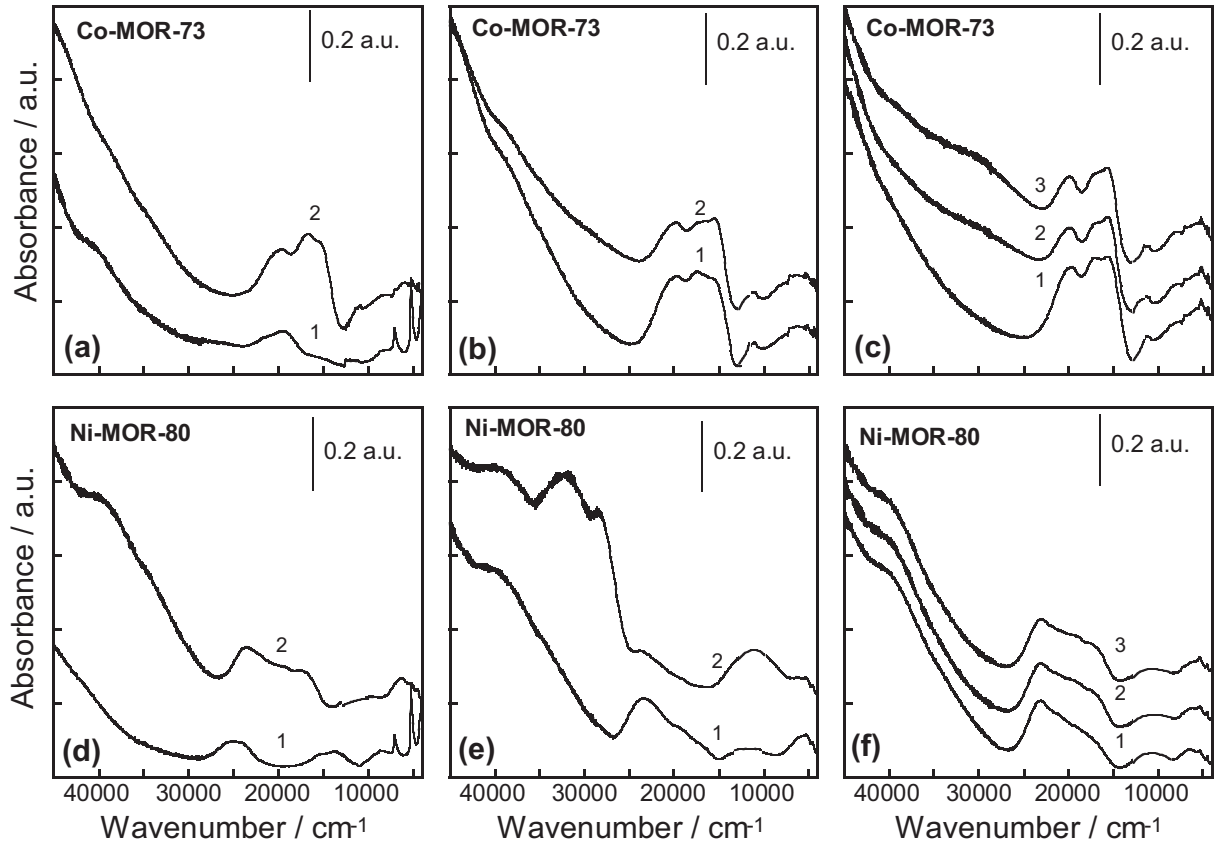

Fig. 9. In situ UV–vis DRS spectra of Co-MOR-73 (Sections a–c) and Ni-MOR-80 (Sections d–f). Sections a and d: samples as prepared under air atmosphere (spectra 1), and standard activated (spectra 2). Sections b and e: samples after adsorption of CO (100 Torr) at RT (spectra 1), and after heating in CO at 623 K and cooling in CO at RT (spectra 2). Sections c and f: samples after adsorption of N_2O (60 Torr) at RT (spectra 1), and after heating in N_2O at 523 K (spectra 2) and 723 K (spectra 3). Spectra are shifted for the sake of clarity.

Ni^{2+}—CO possibly because the Lewis acid strength of Ni^{2+} depends on the number of coordinating framework O atoms and not on the additional coordinating O in extra-lattice position. As for isolated Ni^{2+}—CO, we assign the band at 2212 cm^{-1} on Ni-MOR-80 to carbonyls on Ni^{2+} dimers located mainly in α-sites (type I), and the band at 2207 cm^{-1} on Ni-MOR-20 to carbonyls on Ni^{2+} dimers located in α- and β-sites (type I and type II).

Neglecting the small amount of [Ni^{2+}—O—Ni^{2+}] which underwent reduction at RT on Ni-MOR-80, and assuming that all dimers formed [(CO)—Ni^{2+}—O—Ni^{2+}—(CO)] species and that all reduced at 623 K, the percentage of Ni^{2+} which underwent reduction could be calculated from the percent decrease in the Ni^{2+}—CO band intensity (area/cm^{-1}). Under these hypotheses, we calculated that the amount of reducible Ni^{2+} was at least 30% on Ni-MOR-20 and at least 50% on Ni-MOR-80. Comparing Ni-MOR-80 with Co-MOR-73 having similar tmi-content, the amount of reducible Ni^{2+} (50%) was higher than that of Co^{2+} (about 7% [24]).

3.3. In situ UV–vis DRS characterization

The in situ UV–vis DRS spectra of d–d and charge-transfer transitions have been used to provide information on tmi redox properties and coordination. Spectra of Co-MOR-73 and Ni-MOR-80 samples showed the typical absorptions of tmi complexes without signals of aggregated clusters.

3.3.1. As prepared and standard activated samples.

Spectra taken under air atmosphere of as prepared samples consisted of band due to octahedral tmi^{2+} species: for Co-MOR, Co^{2+} bands at about 8000 and 19,000–22,000 cm^{-1} [41,43,44] (spectra 1 Fig. 9a), and for Ni-MOR, Ni^{2+} bands at about 8700, 14,900 and 24,000 cm^{-1} [43,45] (spectra 1 Fig. 9d). In situ spectra of standard activated samples consisted of bands typical of tmi^{2+} in a distorted tetrahedral configuration: for Co-MOR, Co^{2+} d-d bands in the region 5000–9000 cm^{-1} and 15,000–25,000 cm^{-1} [44,46] (spectra 2 Fig. 9a), and for Ni-MOR, Ni^{2+} d–d bands at about 6300, 11,000 and a multi-component envelop at 15,000–25,000 cm^{-1} [47] (spectra 2 Fig. 9d).

3.3.2. Interaction with CO at increasing temperature

To further investigate the tmi^{2+} reduction process already evidenced by FTIR, the UV–vis DRS spectra of Ni-MOR-80 and Co-MOR-73 were recorded in situ with the same procedure adopted for FTIR CO adsorption experiments reported above (Sections 3.2.2 and 3.2.3).

After exposure to CO at RT, due to CO adsorption, the Co^{2+} d–d bands of standard activated Co-MOR-73 little changed (compare spectrum 2 in Fig. 9a with spectrum 1 in Fig 9b). Heating in CO at 623 K yielded in the region 25,000–33,000 cm^{-1} a weak and undefined absorption, that we assigned to Co^{+} species coordinated with CO (spectrum 2, Fig. 9b).

After exposure to CO at RT, due to CO adsorption, the Ni^{2+} d–d bands of standard activated Ni-MOR-80 little changed (compare spectra 2 in Fig. 9d with spectrum 1 in Fig 9b). Conversely, after heating in CO at 623 K, the band intensity of Ni^{2+} in distorted tetrahedral configuration decreased and an intense band at 11,000 cm^{-1} with a broad doublet at 28,500 and 32,200 cm^{-1} formed (spectrum 2, Fig. 9b). We assign these bands to a tetragonally-distorted octa-

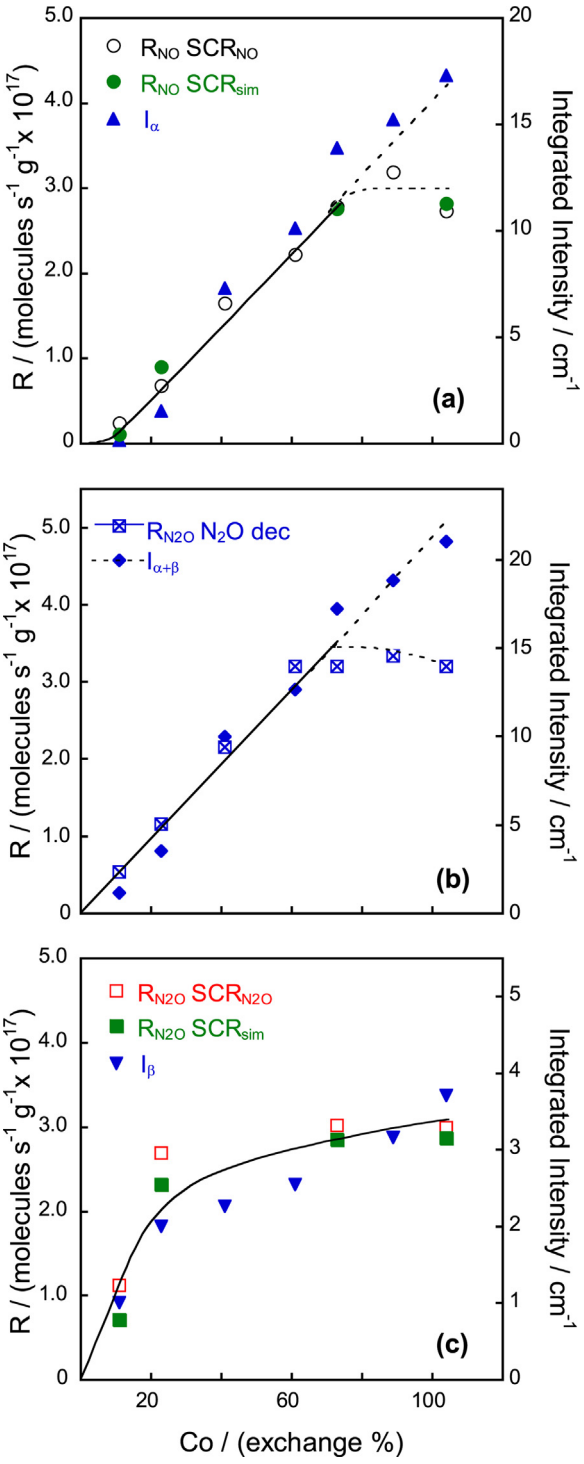

Fig. 10. Correlation between reaction rate (R/molecules s^{-1} g^{-1}) and integrated intensity of carbonyl bands (I/cm^{-1}) on Co-MOR, as a function of Co-exchange percent. Section a: rate of NO abatement in CH_4-SCR_{NO} (○) and CH_4-SCR_{sim} at 673 K (●) and integrated intensity of Co^{2+}—carbonyls in α-site (I_α, ▲); Section b: rate of N_2O decomposition at 623 K (⊠) and the total intensity of Co^{2+}—carbonyls ($I_{\alpha+\beta}$, ♦); Section c: rate of N_2O abatement in CH_4-SCR_{sim} (■) and $CH_4 - SCR_{N_2O}$ at 698 K (□) and the intensity of Co^{2+}—carbonyls in β-site (I_β, ▼). Data for Co-MOR-41, Co-MOR-61 and Co-MOR-89 from [15].

hedral Ni^+—$(CO)_x$ species, in agreement with UV-DRS [48], and EPR characterization [49] of Ni^+—pentacarboxylic acid complex. Kasai et al. [50] suggested that Ni^+—$(CO)_x$ formed by reverse disproportionation of Ni^{2+} and Ni^0, arising during activation. The absence of a continuous background related to the formation of Ni^0 particles [47] in spectra of standard activated Ni-MOR-80, indicated that Ni^+ formed by Ni^{2+} dimers reduction with CO, in agreement with our suggestion by FTIR (see Section 3.2.3).

On both samples, the subsequent standard activation restored the bands of distorted tetragonal tmi^{2+} complexes (spectra not shown for brevity). In agreement with FTIR, DRS confirmed that the amount of reducible $[Ni—O—Ni]^{2+}$ was much higher than that of reducible $[Co—O—Co]^{2+}$.

3.3.3. *Interaction with N_2O at increasing temperature.*

In situ UV–vis–DRS spectra of Co-MOR-73 (Fig. 9c) and Ni-MOR-80 (Fig. 9f) after heating in N_2O were recorded to point out the tmi^{2+} ability to be oxidized.

After exposure to N_2O at RT, the Co^{2+} d–d bands of standard activated Co-MOR-73 did not change (compare spectrum 2 in Fig. 9a with spectrum 1 in Fig 9c). After heating in N_2O at 523 K, a band at about 30,000 cm^{-1} formed (spectrum 2 in Fig. 9c). On increasing heating temperature, the intensity of this band increased (spectrum 3 in Fig. 9c). Band in analogous position was assigned to Co^{3+} [51]. Therefore we assigned this band to Co^{3+}—O^- species formed during N_2O decomposition.

Conversely, after heating in N_2O at increasing temperature up to 723 K, spectra of Ni-MOR-80 were similar to those of standard activated sample (compare spectrum 2 in Fig 9d with spectra 1, 2 and 3 in Fig. 9f), indicating that Ni^{2+} was not oxidized by N_2O.

3.4. *The active site and surface species*

Because Co-MOR and Ni-MOR showed a similar amount and strength of Brønsted acid hydroxyls, Brønsted acidity was not responsible for the difference in their catalytic behavior. Key factors influencing the catalytic activity and directing the reaction pathway were coordination, nuclearity and redox properties of tmi. In MOR, tmi^{2+} can populate sites having different structure and accessibility to gas mixture. Less coordinated sites in the main channels (α-sites) have large 12-membered rings controlling the access (6.5 × 7.0 A), whereas the more coordinated sites in the site pockets (β-sites) have smaller 8-membered rings controlling the access (3.4 × 4.8 A) [16,52].

For Co-MOR, the correlation between Co site-population, evaluated by FTIR quantitative analysis (Fig. 7), and the catalytic activity pattern at increasing Co-content, gave a better insight into the active-site for NO and N_2O abatement reactions. Because all Co-MOR samples had nearly the same value of activation energy for each investigated reaction (data not shown), in each reaction the dependence of rates on the Co-content was the same at all temperatures. At a given temperature, the catalytic activity pattern for NO abatement correlated with the amount of isolated Co^{2+} in α-sites (Fig. 10a). In fact, on increasing Co-exchange extent up to 73%, the rate of NO reduction in both CH_4-SCR_{NO} and CH_4-SCR_{sim} increased in the same way as the amount of Co^{2+}—carbonyls in α-sites (I_α), i.e. they increased little up to 23% and linearly up to 73%. At higher Co-exchange extent, whereas I_α increased further, the rate of NO reduction became constant, due to the presence of Co^{2+} dimers (14% on Co-MOR-104). This correlation confirms our previous results on CH_4-SCR_{NO} and extends to CH_4-SCR_{sim} the suggestion that isolated Co^{2+} located in α-sites are the active sites for NO abatement [15,24].The inactivity of Co^{2+} in β-sites can be ascribed to their low accessibility and steric hindrance to form intermediates (namely nitrites/nitrates and/or $C_xH_yO_zN_k$) [16,18,53].

As concerns N_2O abatement in the simultaneous abatement on Co-MOR, the catalytic results on Co-MOR indicated that N_2O reduction to N_2 occurred via N_2O decomposition up to 650 K, and at higher temperature in little amount via $CH_4 - SCR_{N_2O}$. In agreement with our previous results [25], the active sites for N_2O decomposition were isolated Co^{2+} in α- and β-sites (Fig. 10b). In

fact, on increasing Co-exchange extent up to about 70%, the rate of N_2O decomposition linearly increased as total amount of isolated Co^{2+} located in α- and β-sites ($I_{\alpha+\beta}$). At higher Co-exchange extent, whereas $I_{\alpha+\beta}$ linearly increased further, the rate of N_2O decomposition became constant, due to the presence of $[Co—O—Co]^{2+}$ species (Fig. 10b). The Co^{2+} dimers were inactive because they stabilized oxygen in a strong oxidic form, $[(O^{2-})\cdots Co^{3+}—O—Co^{3+}]$ that not react with N_2O, whereas the active site (isolated Co^{2+}) formed $Co^{3+}—O^-$ by interaction with N_2O [21]. The formation of this species was confirmed by DRS characterization (Section 3.3.3).

As concerns N_2O abatement in $CH_4 - SCR_{N_2O}$, on increasing Co-exchange extent, the rate of N_2O reduction increased in a similar way as isolated Co^{2+} in β-sites (Fig. 10c). The α-sites were inactive for $CH_4 - SCR_{N_2O}$ probably because poisoned by the species formed from activated CH_4. These species did not form in β-sites for steric hindrance. This suggestion requires further spectroscopic investigation.

Also in CH_4-SCR_{sim} on increasing Co-exchange extent, the rate of N_2O abatement increased in a similar way of isolated Co^{2+} in β-sites (Fig. 10c). Since the N_2O abatement in CH_4-SCR_{sim} consisted of decomposition and in a negligible amount of reduction with CH_4, we hypothesize that also N_2O decomposition, as $CH_4 - SCR_{N_2O}$, occurred on β-sites, because α-sites were occupied by nitrite/nitrate intermediates formed in NO abatement.

Characterization results on tmi nuclearity showed an amount of dimers much higher on Ni-MOR than on Co-MOR. Ni-MOR-80 had lower activity than Co-MOR-73 for the NO abatement in CH_4-SCR_{sim} and in CH_4-SCR_{NO}.We suggest that also in Ni-MOR, as in Co-MOR, the isolated Ni^{2+} species located in α-sites were active, having species in β-sites a steric hindrance to form nitrites/nitrates intermediates.

As concerns N_2O abatement, Ni-MOR were inactive for N_2O decomposition, probably because neither isolated Ni^{2+} nor dimers formed $Ni^{3+}—O^-$ species (DRS evidence). In CH_4-SCR_{sim}, Ni-MOR catalysts could abate N_2O via $CH_4 - SCR_{N_2O}$, for which they were highly active. The ineffectiveness in CH_4-SCR_{sim} for N_2O abatement suggests that the active sites for $CH_4 - SCR_{N_2O}$ could be nickel species in α-sites, that, in the presence of NO, were occupied by nitrite/nitrate intermediate.

The key role of nuclearity and redox properties was evidenced by analyzing the catalytic behavior in CH_4 combustion. Ni-MOR was highly active for the CH_4 combustion, whereas Co-MOR was poorly active (compare Figs. 3 and 4). We suggest that methane reduced $[tmi^{2+}—O—tmi^{2+}]$ dimeric species (more abundant in Ni-MOR than in Co-MOR) to $[tmi^{+}—□—tmi^{+}]$, that can be re-oxidized in the presence of oxygen. The redox couple involving dimers, $[tmi^{2+}—O—tmi^{2+}]/[tmi^{+}—□—tmi^{+}]$, is required for CH_4 activation and the redox couple tmi^{2+}/tmi^{3+} is required for the N_2O activation.

We suggest that N_2O abatement proceeded in a different way on Co-MOR and Ni-MOR. On Co-MOR, isolated Co^{2+}, that oxidized to Co^{3+}-O^- with N_2O, were the active sites for N_2O activation (in decomposition or in reduction). On Ni-MOR, dimeric Ni^{2+} species were the active site in $CH_4 - SCR_{N_2O}$, because, once reduced by methane, they can activate N_2O.

To clarify these suggestions on the nuclearity and redox behavior of active site in both $CH_4 - SCR_{N_2O}$ and in methane combustion further investigations are required.

4. Conclusions

Co-MOR catalysts are active for the simultaneous abatement of NO and N_2O with CH_4 in the presence of excess O_2, whereas Ni-MOR are ineffective, because it did not abate N_2O. The comparison between the catalytic behavior of Co-MOR and of Ni-MOR in CH_4-SCR_{sim} and in related reactions ($CH_4 - SCR_{N_2O}$, CH_4-SCR_{NO}, N_2O decomposition, and CH_4 combustion) clarified some features of the reaction pathway.

To be active for NO abatement in the simultaneous process the activity for CH_4-SCR_{NO} is a prerequisite: on both catalysts the NO abatement occurs via CH_4-SCR_{NO}.

To be active for N_2O abatement in the simultaneous process the activity for $CH_4 - SCR_{N_2O}$ is not a prerequisite: notwithstanding their high activity for $CH_4 - SCR_{N_2O}$, Ni-MOR were inactive for N_2O abatement in CH_4-SCR_{sim}. To be active for N_2O abatement the activity for N_2O decomposition is a prerequisite: notwithstanding their high activity for $CH_4 - SCR_{N_2O}$, on Co-MOR N_2O abatement occurs mainly via N_2O decomposition.

From a fundamental viewpoint, the correlation between catalytic behavior and characterization by in situ FTIR and UV–vis DRS clarifies some key properties of tmi for the simultaneous abatement.

For NO abatement in CH_4-SCR_{sim} and CH_4-SCR_{NO} nuclearity and coordination are key properties: on Co-MOR and Ni-MOR active sites are isolated tmi^{2+} located in α-sites, because those in β-sites have steric hindrance.

For N_2O abatement the redox behavior of tmi is a key property: an oxidative step is required to activate N_2O. On Co-MOR isolated Co^{2+} form $Co^{3+}—O^-$ intermediate (DRS evidence), and then they are active for N_2O decomposition and $CH_4 - SCR_{N_2O}$. In CH_4-SCR_{sim} active sites for N_2O abatement are located in β-sites, while those in α-sites are engaged in the NO abatement. On Ni-MOR, Ni^{2+} no $Ni^{3+}—O^-$ form, but dimers $[Ni^{+}—□—Ni^{+}]$, arisen from reduction of $[Ni^{2+}$-O-$Ni^{2+}]$ with CH_4, can be oxidized, and then they are active for $CH_4 - SCR_{N_2O}$.

Acknowledgements

We gratefully thank Luca Tipaldi for performing some catalytic experiments, and INAIL (B-8/DIPIA/09 ex ISPESL project) for financial support.

References

[1] WMO, WMO Greenhouse Gas Bull. 7 (2011) 1–4.
[2] Brochures of EnviNOx, are available at http://www.uhde.biz
[3] M.A.G. Hevia, J. Pérez-Ramírez, Appl. Catal. B 77 (2008) 248–254.
[4] M. Kögel, R. Mönnig, W. Schwieger, A. Tissler, T. Turek, J. Catal. 182 (1999) 470–478.
[5] J. Pérez-Ramirez, J.M. García-Cortés, F. Kapteijn, M.J. Illán-Gómez, A. Ribera, C. Salinas-Martínez de Lecea, J.A. Moulijn, Appl. Catal. B 25 (2000) 191–203.
[6] R.W. van den Brink, S. Booneveld, M.J.F.M. Verhaak, F.A. de Bruijn, Catal. Today 75 (2002) 227–232.
[7] G.E. Marnellos, E.A. Efthimiadis, I.A. Vasalos, Ind. Eng. Chem. Res. 43 (2004) 2413–2419.
[8] Y. Li, J.N. Armor, Appl. Catal. B 3 (1993) 55–60.
[9] F. Schuricht, W. Reschetilowski, Microporous Mesoporous Mater. 164 (2012) 135–144.
[10] G. Delahay, D. Berthomieu, A. Goursot, B. Coq, in: M.A. Keane (Ed.), Interfacial Applications in Environmental Engineering, 108, Marcel Dekker, New York, 2005, pp. 1–22.
[11] G. Busca, M.A. Larrubia, L. Arrighi, G. Ramis, Catal. Today 107–108 (2005) 139–148.
[12] Y. Traa, B. Burger, J. Weitkamp, Microporous Mesoporous Mater. 30 (1999) 3–41.
[13] M.A.G. Hevia, J. Pérez-Ramírez, Environ. Sci. Technol. 42 (2008) 8896–8900.
[14] M.N. Debbagh, C. Salinas Martínez de Lecea, J. Pérez-Ramírez, Appl. Catal. B 70 (2007) 335–341.
[15] M.C. Campa, I. Luisetto, D. Pietrogiacomi, V. Indovina, Appl. Catal. B 46 (2003) 511–522.
[16] D. Kaucký, A. Vondrová, J. Dědeček, B. Wichterlová, J. Catal. 194 (2000) 318–329.
[17] L.B. Gutierrez, E.E. Miró, M.A. Ulla, Appl. Catal. A 321 (2007) 7–16.
[18] F. Lónyi, H.E. Solt, Z. Pászti, J. Valyon, Appl. Catal. B 150–151 (2014) 218–229.
[19] M.C. Campa, V. Indovina, D. Pietrogiacomi, Appl. Catal. B 111–112 (2012) 90–95.
[20] M.C. Campa, V. Indovina, R. Lauri, D. Pietrogiacomi, Catal. Today 191 (2012) 87–89.
[21] Y. Li, J.N. Armor, Appl. Catal. B 2 (1993) 239–256.

[22] M. Mihaylov, K. Hadjiivanov, D. Panayotov, Appl. Catal. B 51 (2004) 33–42.
[23] D. Pietrogiacomi, M.C. Campa, M. Occhiuzzi, Catal. Today 227 (2014) 116–122.
[24] V. Indovina, M.C. Campa, D. Pietrogiacomi, J. Phys. Chem. C 112 (2008) 5093–5101.
[25] M.C. Campa, V. Indovina, D. Pietrogiacomi, Appl. Catal. B 91 (2009) 347–354.
[26] J.N. Armor, Microporous Mesoporous Mater. 22 (1998) 451–456.
[27] S. Bordiga, C. Lamberti, F. Geobaldo, A. Zecchina, G. Turnes Palomino, C. Otero Areán, Langmuir 11 (1995) 527–533.
[28] M.A. Ulla, L. Gutierrez, E.A. Lombardo, F. Lónyi, J. Valyon, Appl. Catal. A 277 (2004) 227–237.
[29] B.I. Mosqueda-Jiménez, A. Jentys, K. Seshan, J.A. Lercher, Appl. Catal. B 43 (2003) 105–115.
[30] M.J. Rice, A.K. Chakraborty, A.T. Bell, J. Catal. 194 (2000) 278–285.
[31] I. Salla, T. Montanari, P. Salagre, Y. Cesteros, G. Busca, J. Phys. Chem. B 109 (2005) 915–922.
[32] C. Otero Areán, M. Rodriguez Delgado, K. Frolich, R. Bulánek, A. Pulido, G. Fiol Bibiloni, P. Nachtigall, J. Phys. Chem. C 112 (2008) 4658–4666.
[33] C. Otero Areán, A.A. Tsyganenko, E. Escalona Platero, E. Garrone, A. Zecchina, Angew. Chem. Int. Ed. 37 (1998) 3161–3163.
[34] M. Mihaylov, K. Hadjiivanov, Langmuir, 18, (2002), 4376–4383, and Ref. therein.
[35] K.J. Hadjiivanov, H. Knözinger, M. Mihaylov, Phys. Chem. B 106 (2002) 2618–2624.
[36] A.I. Serykh, M.D. Amiridis, J. Phys. Chem. C 111 (2007) 17020–17024.
[37] B.I. Mosqueda-Jiménez, A. Jentys, K. Seshan, J.A. Lercher, J. Catal. 218 (2003) 375–385.
[38] H.A. Aleksandrov, V.R. Zdravkova, M.Y. Mihaylov, P. St Petkov, G.N. Vayssilov, K.I. Hadjiivanov, J. Phys. Chem. C 116 (2012) 22823–22831.
[39] A. Penkova, S. Dzwigaj, R. Kefirov, K. Hadjiivanov, M. Che, J. Phys. Chem. C 111 (2007) 8623–8631.
[40] W.J. Mortier, J. Phys. Chem. 81 (1977) 1334–1338.
[41] J. Dědeček, B. Wichterlová, J. Phys. Chem. B 103 (1999) 1462–1476.
[42] C.J.J. den Ouden, R.A. Jackson, C.R.A. Catlow, M.F.M. Post, J. Phys. Chem. 94 (1990) 5286–5290.
[43] A.B.P. Lever, Inorganic Electronic Spectroscopy, 2nd ed., Elsevier, Amsterdam, 1984, Pag. 508 (for Ni^{2+} complexes) and pag. 481 (for Co^{2+} complexes).
[44] P.J. Smeets, Q. Meng, S. Corthals, H. Leeman, R.A. Schoonheydt, Appl. Catal. B 84 (2008) 505–513.
[45] E. Escalona Platero, G. Spoto, S. Coluccia, A. Zecchina, Langmuir 3 (1987) 291–297.
[46] A.A. Verberckmoes, B.M. Weckhuysen, R.A. Schoonheydt, Microporous Mesoporous Mater. 22 (1998) 165–178.
[47] C. Lepetit, M. Che, J. Phys. Chem. 100 (1996) 3137–3143.
[48] R. Piskorski, B. Jaun, J. Am. Chem. Soc. 125 (2003) 13120–13125.
[49] C. Holliger, A.J. Pierik, E.J. Reijerse, W.R. Hagen, J. Am. Chem. Soc. 115 (1993) 5651–5656.
[50] P.H. Kasai, R.J. Bishop Jr., D. McLeod Jr., J. Phys. Chem 82 (1978) 279–285.
[51] B.M. Weckhuysen, M.G. Uytterhoeven, R.A. Schoonheydt, Zeolites 19 (1997) 180–189.
[52] C. Baerlocher, W.M. Meier, D.H. Olson, Atlas of Zeolite Framework Types, 5th revised ed., Elsevier, Amsterdam, 2001.
[53] J. Dědeček, D. Kaucký, B. Wichterlová, Topics in Catalysis 18 (2002) 283–290.